Machine learning-based design of meta-plasmonic biosensors

with negative index metamaterials

Gwiyeong Moon^{1*}, Jong-ryul Choi^{2*}, Changhun Lee¹, Youngjin Oh³, Kyunghwan Kim⁴, and

Donghyun Kim^{1†}

1 School of Electrical and Electronic Engineering, Yonsei University, Seoul, Korea, 03722

2 Medical Device Development Center, Daegu-Gyeongbuk Medical Innovation Foundation

(DGMIF), 80 Cheombok-ro, Dong-gu, Daegu, Korea, 41061

3 OLED Division, Samsung Display, Asan, Chungcheongnam-do 31454, Korea

4 Department of Biomedical Engineering, Yonsei University, Wonju, Korea, 26493

Abstract: In this work, we explore the performance of plasmonic biosensor designs that integrate

metamaterials based on machine learning algorithms. The meta-plasmonic biosensors were designed

for optimized detection of DNA with a layer of double negative metamaterial modeled by an effective

medium. An iterative transfer matrix approach was employed to generate training and test sets of

resonance characteristics in the parameter space for machine learning. As a machine learning-based

prediction of optical characteristics of a meta-plasmonic biosensor, multilayer perceptron and

autoencoder (AE) were used as an algorithm, while the clustering algorithm was constructed by

dimensional reduction based on AE and t-Stochastic Neighbor Embedding (t-SNE) as well as k-means

clustering. Use of meta-plasmonic structure with analysis based on machine learning has found that

enhancement of detection sensitivity by more than 13 times over conventional detection should be

achievable with excellent reflectance curves. Further enhancement may be attained by expanding the

parameter space.

Keywords: Meta-plasmonics; Surface plasmon resonance biosensing; Metamaterial; Machine learning

* These authors contributed equally to this work.

† Corresponding author: kimd@yonsei.ac.kr

1

1. Introduction

Plasmonic sensors detect resonance shifts when surface plasmon (SP) is excited as a result of target biomolecular interactions. Despite many advantages of plasmonic sensing, plasmonic detection suffers from moderate sensitivity due to the label-free nature. For this reason, most of the research in plasmonic detection has been largely focused on improving sensor characteristics such as sensitivity and limit of detection using various approaches, which include amplification of optical signatures (He et al., 2000; Moon et al., 2010; Moon et al., 2012), phase detection (Halpern et al., 2011; Kabashin et al., 2009; Markowicz et al., 2007; Wu et al., 2004), multimodal integration (Oh et al., 2010; Sepúlveda et al., 2006), localization of electromagnetic waves (Byun et al., 2007; Kim et al., 2009; Lee et al., 2015), and colocalization with interactions (Kim et al., 2017; Kim et al., 2012; Oh et al., 2011; Oh et al., 2014). Enhanced sensor performance is achieved by introducing effective metamaterials to a typical SP resonance (SPR) sensor structure. Metamaterials are often implemented by a double negative (DNG) layer which is characterized with both negative permittivity and permeability. It was shown theoretically that negative index metamaterial in itself can excite and support SP modes (Ishimaru et al., 2005). The possibility of metamaterials to produce improved detection characteristics of SPR biosensors has been explored in the past: most of these studies, however, have been limited either to theoretical analysis (Chen et al., 2012; Prajapati et al., 2013) and measuring a simple ambient or binding interaction model (Kabashin et al., 2009).

In this paper, machine learning techniques are applied to the design of metamaterials for enhanced plasmonic sensor structures, while allowing efficient and robust determination of metaplasmonic structure without extensive experimental or theoretical investigation. Machine learning has drawn significant interests for the possibilities of finding patterns and offering validation in the data that are often too complex and massive for human experts (Henriques et al., 2015; Ioffe et al., 2015; Srivastava et al., 2014). Machine learning techniques have been extended to the detection of biological and chemical compounds (Erzinaab et al., 2020; Guselnikova et al., 2019; Pereira et al., 2019; Reza et al., 2010; Seifert et al., 2016) and were also used to optimize an LED array in mobile plasmonic sensing (Ballard et al., 2017). We explore plasmonic detection characteristics based on DNG metamaterials

using machine learning for enhanced detection sensitivity and resonance characteristics. Considering that metamaterials are not something readily available, we have employed machine learning to screen out underperforming metamaterial designs. As a machine learning-based approach, multilayer perceptron (MLP) and autoencoder (AE) were used as an algorithm to predict and cluster optical characteristics for modeling of a meta-plasmonic biosensor. Although we employ meta-plasmonic structures to achieve improved detection sensitivity, this work is intended to be more than a presentation of novel meta-material structures that may give rise to enhanced SPR detection characteristics: rather, an approach *per se* by which metamaterials may be customized for specific target performance. The results suggest that DNG metamaterials can provide enhanced detection performance by more than an order of magnitude, to a degree that plasmonic single molecule sensing may be more feasible, and simultaneously widen the applicability of machine learning to achieve optical label-free detection.

2. Numerical method and model

2.1 Overall flow

The schematic of metamaterial-based plasmonic biosensors that we consider in this study is shown in Figure 1(a). The overall design process consists largely of two steps, as described in Figure 1(b). The first step involves the pre-processing classical calculation prior to machine learning, which starts with metamaterials using an effective medium with negative-index. Far-field optical characteristics were calculated by iterative application of transfer matrices in what we call iterative transfer matrix algorithm (ITMA). The metamaterial structure was simplified using effective medium theory (EMT). The performance of various detection scenarios was tested with detection of DNA oligomers. The procedure is iterated to generate training and test sets. We have then assigned random variable parameters in the multi-dimensional parameter space spanned by the metamaterial structure. The results were employed to generate both training and test sets for the second step in which machine learning algorithm was applied to predict the performance of metamaterial-based plasmonic biosensors.

2.2 Numerical methods

Consider a metamaterial shown in Figure 1(c) with effective permittivity $\varepsilon_{eff} = \varepsilon'_{eff} + j\varepsilon''_{eff}$ = $(n_{eff} + j\kappa_{eff})^2$ and permeability μ_{eff} , where n_{eff} and κ_{eff} refer to refractive index and absorption coefficient. The metamaterials may consist of underlying 2D periodic structures to give rise to the desired effective index using, for example, the second-order EMT (Haggans et al., 1993; Kim et al., 2007; Lalanne et al., 1998; Moon et al., 2006; Rytov, 1956). The detail of approximate model estimation of the meta-material biosensor described in Supporting Information S1.

2.3 Numerical model for meta-plasmonic detection

The schematic of the numerical model that we used to assess molecular detection with the ITMA is presented in Figure 1(b). The five-layer thin film-based structure consists of buffer ambience $(n_{amb} = 1.33)$ and layers of target binding (n_t) , negative-index effective medium with ε_{eff} , and metal (gold) with $\varepsilon_m = (0.18 + 3j)^2$ on a dielectric glass substrate (SF10, $n_s = 1.723$). The ambience was assumed to be distilled water lacking electrolytes, therefore the influence of ionic strength is negligible and use of other ambient solvents may be handled by a refractive index change in the machine learning algorithm. Effect of ambience on the detection sensitivity is discussed in Supporting Information S2. We have evaluated immobilization of 28-mer single-stranded DNA (ssDNA) and hybridization with complementary ssDNA into double-stranded DNA (dsDNA) as reference biomolecular interactions to assess the performance of metamaterial-based plasmonic biosensors. Immobilized and hybridized DNA oligonucleotides were modeled to form a 9.32-nm thick dielectric film with refractive index $n_t = 1.449$ (ssDNA) and 1.517 (dsDNA) (Elhadj et al., 2004). The reliability of machine learning may be affected by the specific hybridization procedure and environmental uncertainties, which can be predicted by the learning model framework and was shown to be within the typical range of experimental errors (Xue et al., 2019). Control data were obtained as resonance shifts produced on 50-nm thick gold thin film and glass substrate. Incident light is assumed to be monochromatic with $\lambda = 632.8$ nm with the direction of electric field oscillation contained in the plane of incidence. The calculation is based on angle-scanning with p-polarized light incidence varied in $\theta_{in} = 40 \sim 89^{\circ}$.

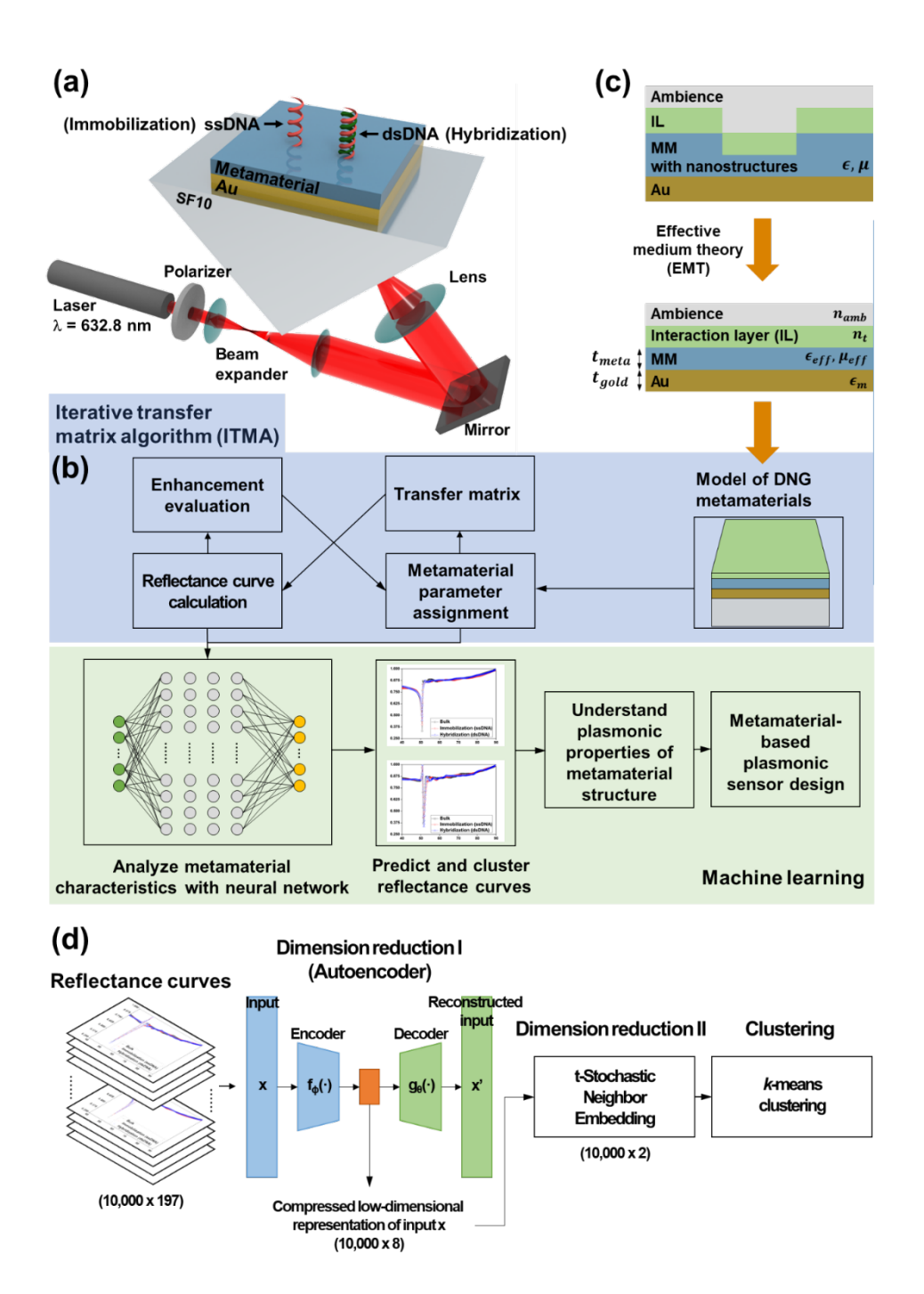


Figure 1 (a) Schematics of metamaterial-based DNA biosensing in immobilization in which 24-mer ssDNA attaches to the metamaterial surface and hybridization of ssDNA to form dsDNA. (b) Workflow of pre-processing classical calculation of metamaterial-based plasmonic detection using simplified effective medium model by the ITMA, which is followed by machine learning for analysis of SPR characteristics. (c) Cross-section of metamaterial-based plasmonic detection of an interaction layer and simplified model using EMT. (d) Machine learning algorithm that consists of three modalities: an AE

to reduce dimensions (10,000 \times 197 \rightarrow 10,000 \times 8) of each reflectance curve, a t-SNE for additional reduction of dimension (10,000 \times 8 \rightarrow 10,000 \times 2) to derive an analytical dimensional level and a k-means clustering for grouping angular reflectance curves.

2.4 Machine learning

The machine learning algorithm is described in Figure 1(b,d) along with the ITMA. The results of the ITMA were fed into the models of machine learning. Detection characteristics of DNA immobilization and hybridization were computed by 375,000 runs in the parameter space. Among these runs, 10,000 data sets were selected for reflection curves and sensitivity enhancement, out of which 8,500 were used for training and 1,500 for the test in the MLP network. The data sets were not divided in the case of using AE, which is unsupervised learning.

MLP network was employed as a method for prediction of reflectance with respect to the incident angle (θ_m). The structure of the MLP network illustrated in Supporting Information S3 consists of functional components of layers: input layer, fully connected (FC), rectified linear unit (Relu), and output layer. Mean squared error (MSE) was used as a loss function in the regression task to train the MLP network. Structure parameters, ε'_{eff} and μ_{eff} , and the metal thickness, t_{gold} , were taken as the input, while angular reflectance was taken as the output of the MLP network. Each of the structure parameters was normalized to range between 0 and 1 for faster learning and reduced likelihood of converging into local minima. Reflection was calculated in $\theta_m = 40 \sim 89^\circ$, at a 0.1° interval, which results in 491 points for each parameter set. Adam, an adaptive learning rate optimization algorithm (Kingma et al., 2014), was employed as the method for stochastic optimization with an initial learning rate of 0.001, a mini-batch size of 85, and the number of epochs at 10,000. The MLP networks were trained separately for the three cases, i.e., bare substrate, DNA immobilization, and hybridization with complementary strands.

Note that AE and t-Stochastic Neighbor Embedding (t-SNE) were also employed to cluster optical characteristic of meta-plasmonic structure and find an appropriate candidate for modeling biosensing by reducing the dimension of reflectance curves and visualizing the data. Visualization with

dimensional reduction allows effective and insightful analysis of high dimensional and big data. AE is an artificial neural network to learn features from unlabeled data and to provide effective representation in the lower dimensional space than the original data (Hinton and Salakhutdinov, 2006). AE consists of two parts: an encoder which maps an input to lower dimensional data and a decoder which reconstructs the input from the lower dimensional data. AE was trained using gradient descent with RMSProp, minibatch size of 100, and the number of epochs of 300. The structure of the AE used in this study is illustrated in Supporting Information S3. t-SNE also performs dimensional reduction by arranging high-dimensional data to be near in the embedding space and allows visualization based on the conversion of distance between data points to joint probability and minimization of the Kullback–Leibler divergence between the joint probabilities (Maaten and Hinton, 2008).

The overall workflow for clustering is illustrated in Figure 1(d). Reflectance curves for bare substrate were used for training AE and calculated for $\theta_{in} = 40 \sim 89^{\circ}$, at a 0.25° interval, which results in 197 points. The primary requirement for intuitive clustering is to lower dimensions of each reflectance curve, for which two consecutive processes using AE and t-SNE were performed. 8,500 reflectance curves in the training data sets with 197 dimensions were compressed to 8 dimensions by AE. Compressed curves by AE were then mapped into 2 dimensions using t-SNE

2.5 Metrics

Meta-plasmonic detection performance was evaluated mainly by sensitivity S, which is defined as $S_{im}^{MM} = (\delta\theta/\delta n)_{immobilization}$ and $S_{hy}^{MM} = (\delta\theta/\delta n)_{hybridization}$. Enhancement En was measured as a ratio of sensitivity using metamaterials to that of conventional detection, i.e., $En_{im} = S_{im}^{MM}/S_{im}^{con}$ and $En_{hy} = S_{hy}^{MM}/S_{hy}^{con}$, where S_{im}^{con} and S_{hy}^{con} represent the sensitivity corresponding to conventional thin film-based detection of DNA immobilization and hybridization. Significant enhancement was defined as the one exceeding an order of magnitude, i.e., En_{im} , $En_{hy} > 10$. For simplification, a geometric average of the enhancement that occurs as a result of DNA immobilization and hybridization is defined as $En = \sqrt{En_{im} \cdot En_{hy}}$ and used as a main performance measure of sensitivity enhancement.

As a quantitative measure of resonance achieved in a meta-plasmonic structure, we have also defined a quality factor α as the difference between reflectance average and minimum at SPR (see Supporting information S4 for rigorous definition of α). Large α may represent good resonance contrast and be an indicator of efficient sensor characteristics.

3. Results and discussion

3.1 Enhancement characteristics of meta-plasmonic detection

Before we explore machine learning approaches, the distribution of En in the parameter space is shown Figure 2(a) with $En > 0 \sim 60$. The histogram of resonance enhancement En produced by metaplasmonic detection of DNA immobilization and hybridization is presented in Figure 2(b). Linearity of detected signals in the dynamic range is important under the experimental circumstances, therefore parameter sets that incur disparate polarity of signals in DNA immobilization and hybridization, i.e., with $En_{im} \cdot En_{hy} < 0$, were excluded. The results clearly confirm that significant enhancement of detection sensitivity by more than 20 times can be produced on DNG metamaterials. For example, when $\varepsilon_{eff} = -1.82957 - 0.001j$ and $\mu_{eff} = -0.866808$ at $t_{meta} = 125$ nm, $E_n = 20.4824$. DNG metamaterials with specific effective parameters can be designed based on metallic hole arrays, double stripes, closed ring resonators, and fishnet structures (Chettiar et al., 2008), as discussed in Supporting Information S5.

3.2 Machine learning based estimation of resonance characteristics

In addition to the sensitivity that *En* represents, resonance characteristics such as reflectance curves serve as a measure of the quality of detection. Because of the prohibitively large amount of data that direct and deterministic investigation of resonance characteristics involves, we have applied machine learning to estimate reflectance curves corresponding to a specific metamaterial-based plasmonic biosensor. In this process, the accuracy of a machine learning platform was also verified. An

estimated reflectance curve was compared with one that was obtained from interpolation of the training data set. For interpolation, we have used nearest interpolation and linear tetrahedral interpolation. Nearest interpolation returns the value of the nearest point in the training set, while, in linear tetrahedral interpolation method, an approximated value is returned by tetrahedralization of the training set (Amidror, 2002). Two measures have been employed to assess quantitative accuracy: a mean-square error (MSE), determined as an average of the difference between an angular reflection response and an error of resonance angle (ERA) which is an average of the difference between resonance angles of exact reflectance and estimated or interpolated result. With more rigorous definition of MSE and ERA that appears in Supporting Information S6, we have assessed MSE and ERA predicted by machine learning (MSE_{ML} and ERA_{ML}) and estimated by nearest (MSE_{Ne} and ERA_{Ne}) and linear tetrahedral interpolation (MSE_{In} and ERA_{In}).

Figure 2(c) shows reflectance curves corresponding to the parameter set $\varepsilon_{eff} = -2.6305$ – 0.001j and $\mu_{eff} = -0.8524$ at $t_{meta} = 70$ nm: exact calculation in black (ITMA), one predicted by MLP in red, and those calculated by the neaerest and the linear tetrahedral interpolation, respectively in blue and green. The reflection curve predicted by MLP resembles exact one, while interpolated curves show visible disparity in the resonance characteristics. MSE and ERA obtained for DNA biosensing in bare control measurements, immobilization, and hybridization using 1,500 parameter sets of metamaterials as test datasets are presented in Figure 2(d) and (e), where average values are shown above the bars with standard deviation provided in Supporting Information S6. The results of MSE compared in Figure 2(d) show clearly that machine learning predicts angular resonance characteristics most accurately. The ratios of MSEs and ERAs suggest that MSE be reduced significantly by an order-of-magnitude with the prediction based on machine learning, while the degree of improvement in accuracy for the case of machine learning is slightly less if measured in terms of ERA. These results were confirmed experimentally using meta-plasmonic structures based on metallic gratings for immobilized probe DNA oligomers (see Supporting Information S7). In other words, prediction of resonance characteristics based on machine learning may well establish the highest accuracy. Between nearest and linear tetrahedral interpolation, the latter performs slightly better in the sense that the MSE is notably lower

while the performance is commensurate in terms of ERA.

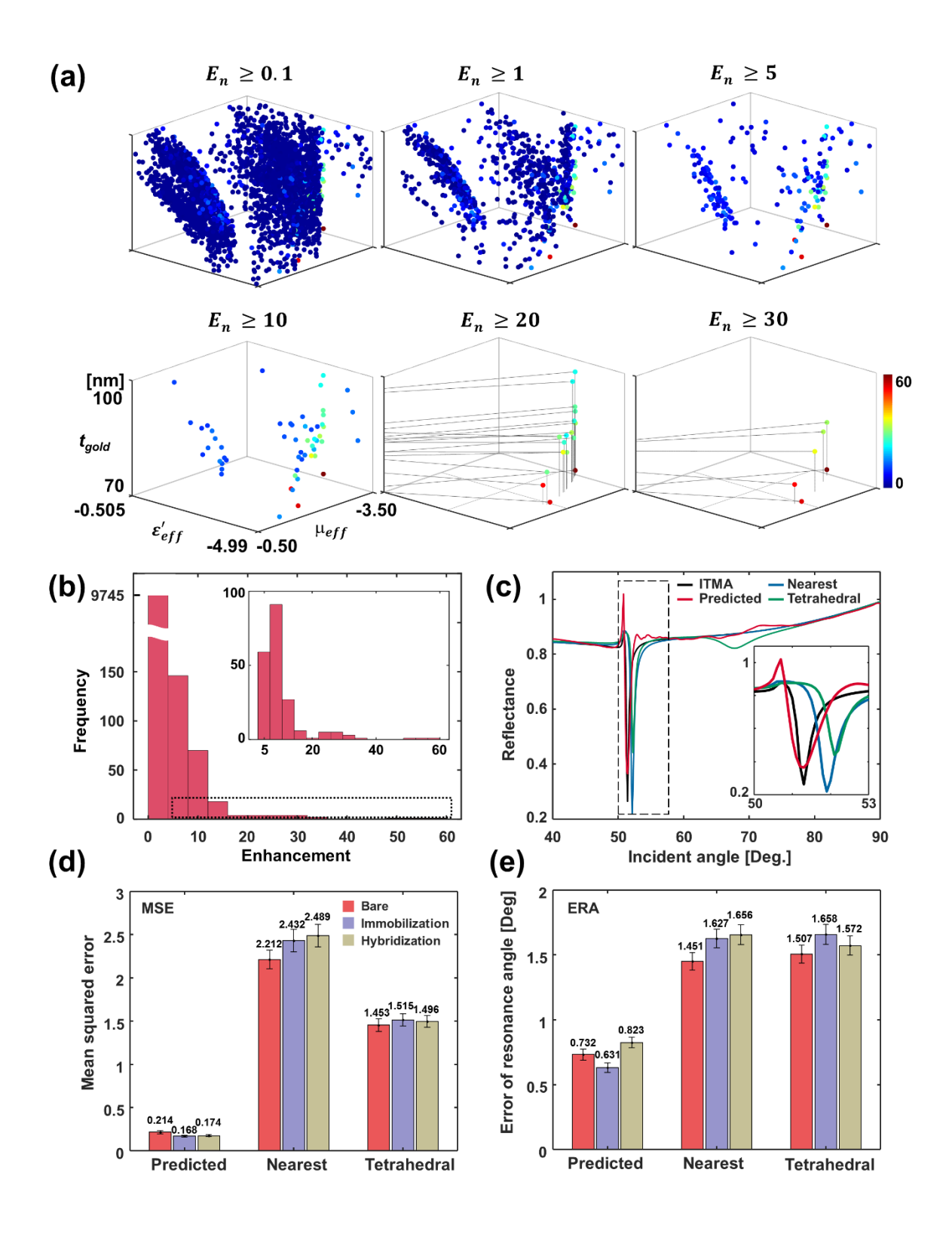


Figure 2 (a) Distribution of En in the parameter space spanned by permittivity (ε'_{eff}), permeability (μ_{eff}), and metal thickness (t_{gold}). (b) Histogram of enhancement En associated with meta-plasmonic

detection. Inset shows magnification of the dotted box for En > 5. (c) Reflectance curves produced with the training data sets using the ITMA (black), prediction with MLP (red), nearest interpolation (green) and linear tetrahedral interpolation. Inset: reflectance magnified around the resonance between $\theta_{in} = 50^{\circ}$ and 53° (d) MSE and (e) ERA of the three methods (MLP and nearest and linear tetrahedral interpolation) for 1,500 test sets. Average values are shown above the bars.

3.3 Clustering of SPR characteristics based on machine learning

The results described in Section 3.1 and 3.2 suggest that the ITMA combined with machine learning may be used to find the parameter sets of metamaterial-based plasmonic biosensors that attain enhanced sensitivity with resonance characteristics tailored to specific patterns. In this section, we apply the algorithm to enforce selectivity, which is often associated with the width of resonance characteristics, in addition to enhanced sensitivity.

With the ITMA, some parameter sets of metamaterials were found to offer an extremely large resonance angle shift, thus exceptionally high detection sensitivity, such as 50 degrees. Oftentimes, the measured shift does not arise from the formation of SP in the range of light incidence and may rather reflect changes of absorption. Therefore, clustering and analysis of reflectance characteristics are required to ensure the resonance to be useful for implementing efficient metamaterial-based biosensors.

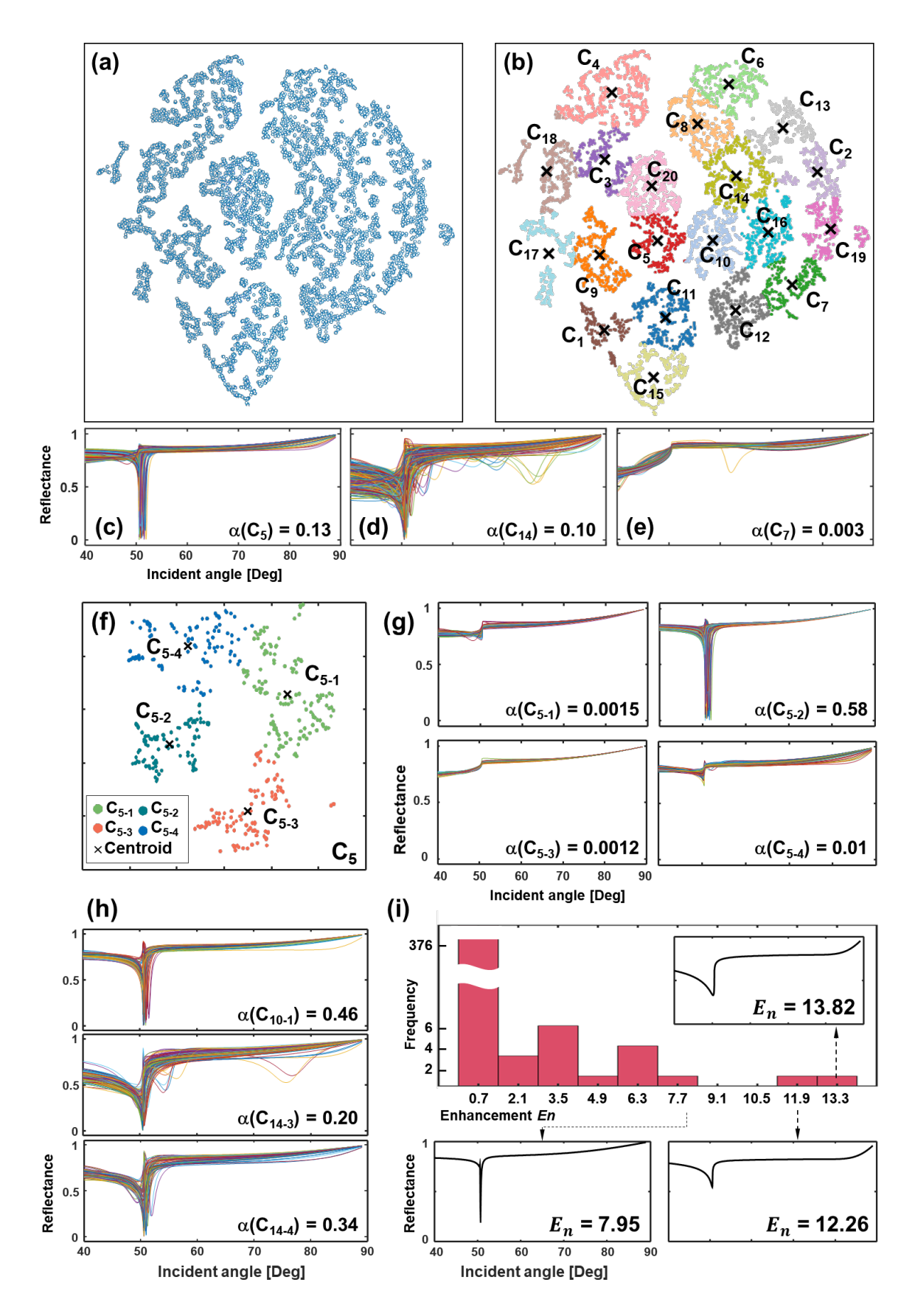


Figure 3 (a) 10,000 reflectance curves mapped into a two-dimensional plane through AE and t-SNE. (b)

Results of k-mean clustering into 20 clusters. The centroids of each cluster are marked with X. (c-e) Reflectance curves corresponding to three clusters taken from (b). (f) Results of k-means clustering of C₅. (g) Reflection curves in subgroup C₅₋₁, C₅₋₂, C₅₋₃, and C₅₋₄. Among the four subgroups, the reflectance curve belonging to C₅₋₂ showed the best SPR characteristics with the largest $\alpha = 0.58$. (h) Reflectance curves in C₁₀₋₁, C₁₄₋₃, and C₁₄₋₄. (i) Histogram of En for the case of C₅₋₂, C₁₀₋₁, C₁₄₋₃, and C₁₄₋₄. Inset presents three reflectance curves that correspond to En = 7.95, 12.26, and 13.82.

Figure 3(a) shows the result of embedding compressed 8 dimensional data in the two-dimensional space by t-SNE. Each point corresponds to one reflectance curve. The distribution of the embedded two-dimensional data points was partitioned into clusters by k-means clustering, which determines a cluster by minimizing the distance between centroids of clusters the data belong to (Lloyd, 1982). Note that the number of groups (k) can be determined by several algorithms (Kodinariya, 2013). Figure 3(b) presents the result after k-means clustering when k was defined as 20, where each cluster is named as C_1 , C_2 , ... and C_{20} . Points which belong to the same cluster are represented in an identical color. Reflectance curves of three clusters C_5 , C_{14} , and C_7 are plotted in Figure 3(c-e). Reflectance curves of C_5 shown in Figure 3(c) tend to have well-defined SPR dips with an average of α in C_5 found to be $\alpha(C_5) = 0.13$. In contrast, reflectance curves of C_{14} in Figure 3(d) were found to have less pronounced resonance characteristics with $\alpha(C_{14}) = 0.1$. On the other hand, C_7 consists of curves with no trace of resonance, as shown in Figure 3(e), with very small α , i.e., $\alpha(C_7) = 0.003$, and thus does not render practical uses as a sensor despite fairly high En. For reference, reflectance curves that belong to other clusters and α are presented in Supporting Information S8.

Note that even C_5 shown in Figure 3(c) contains reflectance curves without well-defined resonance dips. This necessitates secondary clustering, for which we conducted k-means clustering. Figure 3(f) shows the result of k-means clustering for C_5 with k = 4 (see Supporting Information S9 for optimization of k). Each of the secondary clustered groups was named as C_{5-j} ($j = 1 \sim k$). Figure 3(g) presents the reflectance curves of C_{5-j} and it was confirmed that reflectance curves that belong to C_{5-2} show the best SPR features. C_{10} and C_{14} , with SPR features similar to C_5 , were also performed with k-

means clustering for k = 5. Among the subgroups, reflectance curves of C_{10-1} , C_{14-3} , and C_{14-4} , which have well-defined SPR dips and high α , are plotted in Figure 3(h). In total, there were 393 reflectance curves in these groups, including C_{5-2} . En associated with these curves was presented in the histogram in Figure 3(i). Reflection curves with high En are also provided with the highest En reaching 13.82 found in C_{14-3} . The results suggest that highly enhanced detection sensitivity can be obtained while optimizing resonance characteristics based on machine learning algorithm. We emphasize that the machine learning-based procedure described in this study can be used to select and keep only those meta-plasmonic structures that may be practical while achieving sensitivity that is enhanced by more than an order of magnitude over conventional detection.

3.4 Discussion

A machine learning-based approach can be extended beyond the prediction of the performance in terms of sensitivity enhancement and resonance characteristics. For example, the algorithm may reflect fabrication of a metamaterial-based biosensor design. Note that metamaterials have been constructed with, for instance, split-ring resonators (Gwinner et al., 2009; Papasimakis et al., 2010; Tobing et al., 2014), helical nanostructures (Johannes and Wegener, 2016), and multilayer fishnet structures (García-Meca et al., 2011; Jia and Wang, 2019; Valentine et al., 2011), which can be considered in the design process. Also, wider ranges of metamaterial parameters can be studied to achieve higher sensitivity enhancement. Another metric to use is the robustness or tolerance of a parameter set, i.e., a large volume of a group in the parameter space, with which sensitivity exceeds a target, makes a design immune to fabrication errors.

One may wonder about the case without machine learning. We stress that machine learning-based design principles allow extraction of features for required task and show highly adaptive class of objects. Even in conventional methods without machine learning, a massive search in the full parameter space may eventually find an optimum set of parameters with which the sensor performance may reach an optimum. With machine learning, optimum parameter sets can be found without consuming much computational resources in an N dimensional parameter space (N >> 3) as well as more systematic

understanding of feature effects.

4. Conclusions

In this study, we report machine learning-based design of metamaterials for highly sensitive SPR biosensing. After classical calculation using ITMA to generate training and test data sets, machine learning was performed sequentially in two layers, to explore optimal detection sensitivity for DNA and to achieve SPR characteristics for applications in practice. By evaluating the error in terms of MSE and ERA, machine learning produced much smaller error with higher accuracy for prediction of reflectance curves and resonance angles than interpolation methods. The clustering algorithm was constructed by dimensional reduction based on AE and t-SNE as well as *k*-means clustering. Machine learning was shown to allow use of metamaterial to improve the detection sensitivity by more than 13 times over conventional SPR biosensing with useful resonance characteristics. The results can be extended to achieving desired optical characteristics beyond metamaterial-based SPR biosensors.

Acknowledgment

This work was supported by the National Research Foundation (NRF) grants (NRF-2019R1A4A1025958, 2019R1F1A1063602, and 2019K2A9A2A08000198) funded by the Korean Government. Part of this work was performed on sabbatical at UC Irvine, supported by NSF CHE 1856165. Authors thank Prof. Kieron Burke at Department of Chemistry of UC Irvine for insightful discussion in this work.

References

Amidror, I., 2002. J. Electron. Imaging 11, 157-176.

Ballard, Z.S., Shir, D., Bhardwaj, A., Bazargan, S., Sathianathan, S., Ozcan, A., 2017. ACS Nano 11, 2266-2274.

Byun, K. M., Yoon, S. J., Kim, D., Kim, S. J., 2007. Opt. Lett. 32, 1902-1904.

Chen, T., Li, S., Sun, H., 2012. Sensors 12, 2742–2765.

Chettiar, U. K., Xiao, S., Kildishev, A. V., Cai, W., Yuan, H. K., Drachev, V. P., Shalaev, V. M., 2008. MRS Bullet. 33, 921-926.

Elhadi, S., Singh, G., Saraf, R. F., 2004. Langmuir 20, 5539-5543.

Erzinaab, M., Trelin, A., Guselnikova, O., .Dvorankov, B., Strnadova, K., Perminova, A., Ulbrich, P., Mares, D., Jerabek, V., Elashnikov, R., Svorcik, V., Lyutakov, O., 2020. Sens. Actuators B 308, 127660.

García-Meca, C., Hurtado, J., Martí, J., Martínez, A., Dickson, W., Zayats, A. V., 2011. Phys. Rev. Lett. 106, 067402.

Guselnikova, O., Trelin, A., Skvortsova, A., Ulbrich, P., Postnikov, P., Pershina, A., Sykora, D., Svorcik, V., Lyutakov, O., 2019. Biosens. Bioelectron. 145, 111718.

Gwinner, M. C., Koroknay, E., Fu, L., Patoka, P., Kandulski, W., Giersig, M., Giessen, H., 2009. Small 5, 400–406.

Haggans, C. W., Li, L., Kostuk, R. K., 1993. J. Opt. Soc. Am. A 10, 2217–2225.

Halpern, A. R., Chen, Y., Corn, R. M., Kim, D., 2011. Anal. Chem. 83, 2801–2806.

He, L., Musick, M. D., Nicewarner, S. R., Salinas, F. G., Benkovic, S. J., Natan, M. J., Keating, C. D., 2000. J. Am. Chem. Soc. 122, 9071–9077.

Henriques, J. F., Caseiro, R., Martins, P., Batista, J., 2015. IEEE Trans. Pattern Anal. Mach. Intell. 37, 583-596.

Hinton, G. E., Salakhutdinov, R. R., 2006. Science 313 (5786), 504-507.

Ioffe, S., Szegedy, C., 2015. arXiv preprint arXiv 1502, 03167.

Ishimaru, A., Jaruwatanadilok, S., Kuga, Y., 2005. Prog. Electromagn. Res. 51, 139–152.

Jia, X., Wang, X., 2019. Optik 182, 464–468.

Johannes, K., Wegener, M., 2016. Nanophotonics 5, 510–523.

Kabashin, A. V., Evans, P., Pastkovsky, S., Hendren, W., Wurtz, G.A., Atkinson, R., Pollard, R., Podolskiy, V. A.,

Zayats, A. V., 2009. Nat. Mater. 8, 867–871.

Kim, D., Yoon, S. J., 2007. Appl. Opt. 46, 872-880.

Kim, K., Kim, D. J., Moon, S., Kim, D., Byun, K. M., 2009. Nanotechnology 20, 315501.

Kim, K., Lee, W., Chung, K., Lee, H., Son, T., Oh, Y., Xiao, Y.-F., Kim, D. H., Kim, D., 2017. Biosens. Bioelectron. 96, 89–98.

Kim, Y., Chung, K., Lee, W., Kim, D. H., Kim, D., 2012. Appl. Phys. Lett. 101, 233701.

Kingma, D. P., Ba, J., 2014. arXiv preprint arXiv1412, 6980.

Kodinariya, T. M., Makwana, P. R., 2013. Int. J. Adv. Res. Compute. Sci. Manag. Stud. 1, 90–95.

Lalanne, P., Hugonin, J. P., 1998. J. Opt. Soc. Am. A 15, 1843–1851.

Lee, W., Kinosita, Y., Oh, Y., Mikami, N., Yang, H., Miyata, M., Nishizaka, T., Kim, D., 2015. ACS Nano 9, 10896–10908.

Lloyd, S., 1982. IEEE Trans. Inf. Theory 28, 129-137.

Maaten, L. V. D., Hinton, G., 2008. J. Mach. Learn. Res. 9, 2579-2605.

Markowicz, P. P., Law, W. C., Baev, A., Prasad, P. N., Patskovsky, S., Kabashin, A., 2007. Opt. Express 15, 1745–1754.

Moon, S., Kim, D., 2006. J. Opt. Soc. Am. A 23, 199-207.

Moon, S., Kim, D. J., Kim, K., Kim, D., Lee, H., Haam, S., 2010. Appl. Opt. 49, 484-491.

Moon, S., Kim, Y., Oh, Y., Lee, H., Kim, H. C., Lee, K., Kim, D., 2012. Biosens. Bioelectron. 32, 141–147.

Oh, J., Chang, Y. W., Yoo, S., Kim, D. J., Im, S., Park, Y. J., Kim, D., Yoo, K.-H., 2010. Nano Lett. 10, 2755–2760.

Oh, Y., Lee, W., Kim, D., 2011. Opt. Lett. 36, 1353-1355.

Oh, Y., Lee, W., Kim, Y., Kim, D., 2014. Biosens. Bioelectron. 51, 401–407.

Papasimakis, N., Luo, Z., Shen, Z. X., de Angelis, F., di Fabrizio, E., Nikolaenko, A. E., Zheludev, N. I., 2010. Opt. Express 18, 8353–8359.

Pereira, V. R., Pereira, D. R., de Melo Tavares Vieira, K. C., Ribas, V. P., Constantino, C. J. L., Antunes, P. A.,

Favareto, A. P. A., 2019. Environ. Sci. Pollut. Res. 26, 35253-35265.

Prajapati, Y. K., Yadav, A., Verma, A., Singh, V., Saini, J.P., 2013. Optik 124, 3607–3610.

Nezhad, M. R. H., Tashkhourian, J., Khodaveisi, J., Khoshi, M. R., 2010. Anal. Methods 2, 1263-1269.

Rytov, S. M., 1956. Sov. Phys. J. Exp. Theor. Phys. 2, 466–475.

Seifert, S., Merk, V., Kneipp, J., 2016. J. Biophoton. 9, 181-189.

Sepúlveda, B., Calle, A., Lechuga, L. M., Armelles, G., 2006. Opt. Lett. 31, 1085–1087.

Srivastava, N., Hinton, G., Krizhevsky, A., Sutskever, I., Salakhutdinov, R., 2014. J. Mach. Learn. Res. 15, 1929–1958.

Tobing, L.Y., Tjahjana, L., Zhang, D. H., Zhang, Q., Xiong, Q., 2014. Adv. Opt. Mater. 2, 280–285.

Valentine, J., Zhang, S., Zentgraf, T., Zhang, X., 2011. Proc. IEEE 99, 1682–1690.

Wu, S. Y., Ho, H. P., Law, W. C., Lin, C., Kong, S. K., 2004. Opt. Lett. 29, 2378–2380.

Xue, Y., Cheng, S., Li, Y., Tian, L., 2019. Optica, 6, 618-629.